 ICCES, vol.9, no.4, pp.247-261

Coarse-grained molecular dynamics simulation on Cu (100) nano-indentation

Tei-Chen Chen[1,2], Heng-Chieh Wang[1], Shu-Fan Wu[1], Yen-Hung Lin[1]

Summary

Mechanical properties of materials in the micro- and nano-meter scale have been successfully obtained by using the indentation technique. Up to now, large-scale atomistic models to simulate the experimental condition, however, still remain computationally demanding. In this article, a simple and accurate method is proposed to derive the intermolecular potential functions of coarse-grained molecular dynamics (CGMD) suitable for various single crystalline materials. This CGMD technique is then provided to simulate nano-indentation process to verify its accuracy and reliability. Simulation results evaluated by CGMD approach are obtained and compared to those predicted by MD. It is found that the results predicted by these two approaches are well consistent in various aspects such as the deformation patterns, the force-displacement curves as well as the Young's modulus and the hardness. Moreover, the computational time of CGMD can be saved significantly. It takes only about one-fifth in comparison to MD. Consequently, this methodology can be utilized to simulate larger systems with more atoms required in various nanometer-scale processes.

keywords: Coarse-grained molecular dynamics, multi-scale, finite element method, nano-indentation.

Introduction

State-of-the-art atomistic molecular-dynamics simulations are capable of dealing with the system up to millions of atoms by using advanced parallel computer architectures. However, a significant gap in size-scale still exists and needs to bridge between atomistic simulation and experiment. For instance, a MD simulation on indentation-induced structural phase transformations in mono-crystalline silicon using very large cell has been conducted recently by Kim and Oh [1]. In their model the substrate consisted of about 1.6×10^6 silicon atoms in total with a size of 38 nm $\times$ 38 nm $\times$ 21 nm. The maximum indentation depth has reached to 7.5 nm. Although long-range crystalline order and the mechanism of overall phase transformation within the subsurface have been obtained in this study, the maximum indentation depth in simulation, however, was still less than the experimental data by two to three orders in magnitude.

Consequently, a large-scale atomistic model to approximate the experiment condition still remains computationally demanding. Some alternatives that com-

[1]Department of Mechanical Engineering, National Cheng Kung University, Tainan 701, Taiwan
[2]Corresponding author. Email:ctcx831@mail.ncku.edu.tw

bine atomistic simulation with coarse-grained scheme have been resorted to. Quasi-continuum (QC) method, based on a zero-temperature energy minimization technique, is one of main trends [2-6]. In this method an approximation to the total potential energy is obtained by using finite element constraints to remove atoms where the deformation field varies slowly on the scale of lattice parameter. Not only the total number of degrees of freedom that must be considered to simulate the deformation of the system can be significantly reduced, but also an attractive feature of seamlessness can be achieved. In other words, the same underlying atomistic model can be used in both the coarse-grained and fully-atomistic regions. Although QC method can simulate nano-indentation process up to several tens of nanometers, many disadvantages, however, may be introduced due to simple and unrealistic phenomenological constitutive models. Moreover, this approach cannot capture the important features of experimental results in atomistic aspects such as defect formation and hysteretic loop.

In the past decade a number of hybrid atomistic continuum schemes have been developed. Tadmor et al. [7, 8] first proposed the concept of finite-element coarse graining to investigate the quasi-static propagation of defects in crystalline solids. In their procedures the atoms underlying a given element moved instantaneously in unison with the nodes of that element. The temperature was implicitly assigned to zero K and then the potential energy of the system was minimized under specified boundary conditions to yield the optimal static nodal configuration and an estimation of the configuration energy of the stable state. On the other hand, Rudd and Broughton [9, 10] proposed a coarse-grained molecular dynamics (CGMD) based on finite-element technique. In their theory, the coarse-grained Hamiltonian is dependent on temperature, containing a term representing the mean thermal energy of non-nodal atoms introduced due to the loss of degrees of freedom in coarse graining. Some studies [11-12] proposed an alternative static finite-element coarse-graining description, which was an extension to nonzero temperature of the static coarse-graining approach of Tadmor et al. It was found that minimization of Helmholz energy functional will lead to the optimal static nodal configuration and the best estimation of the Helmholz energy under the given boundary conditions. This extended quasi-continuum technique can yield the exact solution if it was applied to pure one-dimensional harmonic chain [11]. Chao et al. [13] proposed a coarse-grained multi-scale molecular simulation method, called coarse-grained rigid blob model, for soft matter systems that directly incorporated stereochemical information. In this method the material was divided into disjoint groups of atoms or particles, called rigid blobs, which moved as separate rigid bodies. The construction of transferable interblob potentials that approximated the net intermolecular interactions was obtained by utilizing a multi-polar expansion technique.

The potential energy of CGMD is generally constructed by taking Taylor series expansion of intermolecular potential function. Since only few terms are included for saving computational effort, these two potential functions only match well near equilibrium position. In other words, only the region with small deformation can be accurately simulated by CGMD. In this study, a simple CGMD approach suitable for mono-crystalline materials is proposed. Intermolecular potential functions for different size-scale of CGMD with the same lattice structure as atoms can be easily obtained theoretically instead of determining by taking Taylor series expansion. Consequently, accurate results can also be obtained even using larger size-scale of CGMD

Theory of CGMD

CGMD Hamiltonian

In this article, a method of constructing scale-dependent constitutive equations suitable for different meshes, quite similar to the method of Rudd et al. [9], is proposed and developed. In the regions where the mesh nodes and the atomistic sites are identical the CGMD equations of motion should agree with the atomistic equations of motion. In other words, this enables MD regions to be coupled seamlessly to the regions of CGMD and the interfacial handshaking regions become unnecessary. The displacement of mesh node j in CGMD is an average of the atomistic displacements within this mesh

$$u_j = \sum_{\mu} f_{j\mu} u_{\mu}, \tag{1}$$

where $f_{j\mu}$ is a weighting function, related to the finite element interpolating functions. Similar relation can be found for the momenta $\mathbf{p}_{\mu}$. By the definition of interpolating functions, the weighting function, $f_{j\mu}$, can then be derived in terms of shape functions

$$f_{j\mu} = \sum_{k} \left(\sum_{\nu} N_{j\nu} N_{k\nu} \right)^{-1} N_{k\mu}, \tag{2}$$

where $N_{k\mu} = N_k(x_{\mu})$. It should be noted that Latin indices, j, k, denote mesh nodes while Greek indices, μ, ν, denote atoms. The CGMD energy can be defined as the average of the canonical ensemble of the constrained phase space such that the position and momentum of the atoms are consistent with the mean displacement and momentum fields and can be written as [9]

$$E\left(u_k, \dot{u_k}\right) = \langle H_{MD} \rangle_{u_k, \dot{u_k}} = \int dx_{\mu} dp_{\mu} H_{MD} e^{-\beta H_{MD}} \Delta / Z, \tag{3}$$

where $\Delta = \prod_j \delta \left(u_j - \sum_{\mu} u_{\mu} f_{j\mu} \right) \delta \left(\dot{u}_j - \sum_{\mu} \frac{p_{\mu} f_{j\mu}}{m_{\mu}} \right)$, $\delta(\mathbf{u})$ is a three-dimensional delta function; Z is the partition function; $\beta = (kT)^{-1}$ is the inverse temperature (energy).

The atomistic Hamiltonian can be expressed in the form

$$H_{MD} = \sum_{\mu} \frac{p_{\mu}^2}{2m} + V_{MD}, \tag{4}$$

where $V_{MD} = \sum_{\mu,\nu} V_{\mu\nu}$.

The mass matrix of CGMD can be derived by using the inverse matrix

$$E\left(u_k, \dot{u}_k\right) = U_{int} + \sum_{j,k} \frac{1}{2} M_{jk} \dot{u}_j \cdot \dot{u}_k + V_{CGMD}, \tag{5}$$

where $U_{int} = 3(N_{MD} - N_{CGMD})kT$; $M_{jk} = m\left(\sum_{\mu} f_{j\mu} f_{k\mu}\right)^{-1}$; $V_{CGMD} = V_{MD} = \sum_{j,k} V_{jk}$.

It is obvious that the equations of motion for CGMD are identical to those of MD in the regions where the mesh coincides with the atomistic sites.

Potential function of CGMD

The relationship of potential functions between CGMD and MD analysis should be identical, i.e.,

$$\sum_{\mu,\nu} V_{\mu\nu} = \sum_{j,k} V_{jk}. \tag{6}$$

In the present study, the construction of CGMD potential functions between Cu atoms are obtained by using the tight–bonding potential theory, proposed by Cleri and Rosato [14], and Morse potential [15], respectively. The tight-binding potential, E_c, mainly composed of two terms, i.e. bonding terms, E_B^i, and repulsive energy term, E_R^i, can be expressed as

$$E_C = \sum_i \left(E_B^i + E_R^i\right), \tag{7}$$

where

$$E_B^i = -\left\{\sum_j \xi^2 e^{-2q\left[r_{ij}/r_0\right]}\right\}^{1/2}, \tag{8}$$

$$E_R^i = \sum_j A e^{-p\left(r_{ij}/r_0\right)}, \tag{9}$$

in which r_0 is the equilibrium distance between molecules; A, p, ξ and q are four key parameters which are determined by experiments [14].

The Morse potential, $\Phi(r)$, which is popularly adopted in solid, can be written as

$$\Phi(r) = D\left\{e^{-2\alpha(r-r_0)} - 2e^{-\alpha(r-r_0)}\right\}, \tag{10}$$

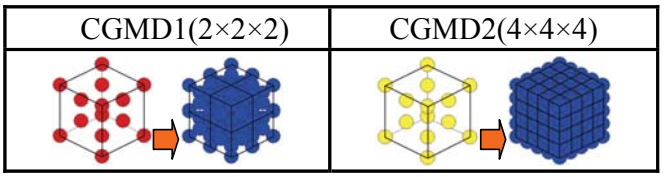

(a)

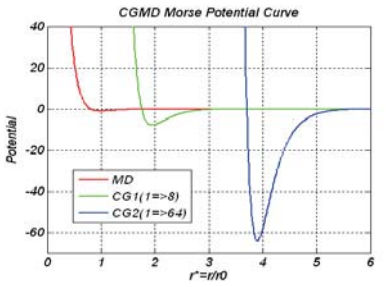

(b)

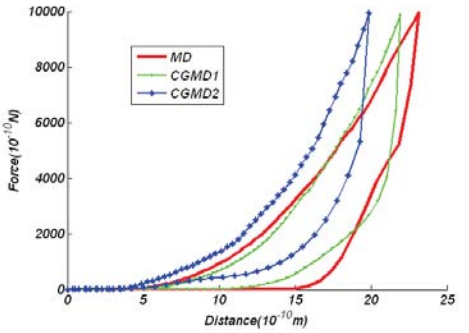

(c)

Figure 1: (a) Lattice structures of CGMD; (b) All atomic and CGs potentials and (c) Force vs. indentation depth curves for all-atom MD and CGMD simulation models

where the parameter D is the coherent energy; α is the material parameter; r_0 is the equilibrium distance and can be determined by spectrum data.

In general, the parameters of potential function for different size-scale of CGMD should be determined through either Taylor series expansion of potential function or curve fitting by comparing to the potential function of all-atom model under the same deformation condition. In this article, a simple approach is adopted. As shown in Fig. 1(a), two different CGMD lattices are adopted in atomic simulation. $2 \times 2 \times 2$ and $4 \times 4 \times 4$ lattices of atoms in FCC structure are individually replaced by 1 lattice of CGMD1 and CGMD2, respectively. In other words, each node in CGMD1 and CGMD2 lattices is equivalent to 8 and 64 atoms, respectively. It is found that if CGMD keeps the same FCC lattice structure as the all-atom model, sound structural stability can be achieved in all the regions especially near the interfaces between different meshes. Consequently, the Morse potential for CGMD1 and CGMD2 lattices can be, respectively, expressed as:

$$\Phi(r) = 8D\left\{e^{-2\cdot\alpha\cdot(r-r_{01})} - 2e^{-\alpha\cdot(r-r_{01})}\right\}, \tag{11}$$

$$\Phi(r) = 64D\left\{e^{-2\cdot\alpha\cdot(r-r_{02})} - 2e^{-\alpha\cdot(r-r_{02})}\right\}, \tag{12}$$

where r_{01} and r_{02} represent the equilibrium distance for CGMD1 and CGMD2 lattices, respectively. It can be easily shown that under the condition of uniform

deformation Eq. (6) is satisfied if $r_{01} = 2r_0$ and $r_{01} = 4r_0$, while the other two parameters, D and α remain unchanged for CGMDs with two different sizes, respectively. Consequently, the data of these parameters, corresponding to all-atom, CGMD1, and CGMD2, for Morse and tight-binding potentials are listed in Tables 1 and 2, respectively. The potential functions of CGMD1 and CGMD2 are plotted in Fig. 1(b). Moreover, indentation simulations for the systems, composed of pure CGMD1 and CGMD2 lattices, are carried out, respectively. Their indentation load and displacement curves are plotted and compared to the case of all atoms, as shown in Fig. 1 (c). It can be found that the simulation results are quite consistent. However, numerical results of CGMD show a little harder stiffness than all-atom; and the larger the size of CGMD, the harder the stiffness.

Table 1: Data of parameters in Morse Potential

Parameter	MD (Cu-Cu)	MD (C-Cu)	CGMD1(2×2×2) (Cu-Cu)	CGMD2(4×4×4) (Cu-Cu)
D(eV)	0.3429	0.1	0.3429	0.3429
$\alpha(^{-1})$	1.3588	1.7	1.3588	1.3588
r_0()	2.626	2.2	5.252	10.504

Table 2: Data of parameters in Tight-Binding Potential

Parameter	MD (Cu-Cu)	CGMD1(2×2×2) (Cu-Cu)	CGMD2(4×4×4) (Cu-Cu)
A(eV)	0.0855	0.0855	0.0855
P	10.96	10.96	10.96
ζ(eV)	1.224	1.224	1.224
q	2.278	2.278	2.278
r_0()	2.5662	5.1324	10.2648

Table 3: Hardness and Young's modulus estimated by four different models

	Experimental [19]	MD (Morse)	CGMD (Morse)	MD (TB)	CGMD (TB)
Hardness (GPa)	10	13.8	14.7	10.5	11.5
Young's modulus (GPa)	135	275	263	302	289

Simulation methodology

The simulation model is composed of single crystalline (100) Cu substrate and a diamond indenter. In order to demonstrate the accuracy and reliability of CGMD, both the models of all-atom and CGMD are adopted in the present study. As shown in the Fig. 2, the size of substrate is 145Å× 145 Å× 94Å, and a Berkovich diamond indenter with cone angle of 130^o is composed of 15212 carbon atoms. For all-atom MD model, the substrate is composed of 166400 Cu atoms. A model with different lattices, called the CGMD model, is also adopted in simulation. This model is com-

posed of 38400 atoms, 6400 small CGMD1 nodes and 1200 large CGMD2 nodes, totally 45600 particles. Atoms are arranged on the upper side of the system that is deformed severely; while small and large CGMDs are respectively imposed on the central and lower sides of the system with small deformation. Selection of suitable potential functions is very important to ensure reliable results in this indentation process. For all-atom model, tight-binding potential and Morse potential are used to depict the interaction between Cu atoms in substrate, respectively; while Morse potential is used between the Cu atoms in the substrate and the carbon atoms in the indenter. On the other hand, tight-binding potential and Morse potential are also used to describe the interaction between small CGMD nodes, as well as between large CGMD nodes, respectively. The techniques of embedded pseudo particles and representative particles are adopted to treat the interactions near the interfaces between atom and small CGMD, as well as between small and large CGMDs. For instance, to evaluate the forces acted on the atom by small CGMD particles near the interface between the atom and the small CGMD nodes, embedded pseudo atoms within the region of cut-off radius for this atom are located first; and then the interactions between the real and pseudo atoms are evaluated by using the potential function between atoms. Consequently, potentials between atoms, as well as between the same CGMD nodes can be adopted directly to keep from the numerical instability encountered by mixed rule. To restrict the rigid-body motion of substrate, atoms at bottom layer are fixed, while the remaining layers are thermal control layers to impose the substrate temperature. In this work, the simplest way to control the temperature of the system is adopted. This method just scales the velocities at each time step to keep the time average of the total kinetic energy of the system in correspondence with the desired substrate temperature. Moreover, periodic boundary conditions (PBC) are imposed on the four lateral surfaces. The indentation process is performed by moving down the indenter at the speed of 300 m/s at a temperature of 300 K under the maximum loading of 1000 nN. The 5^{th}-order Gear algorithm of the time integration method with time step 1 fs is used in this study. H-functions [16] are used to monitor the equilibrium of the system. It is found that the systems with mixed lattices take 12000 and 15000 steps to reach equilibrium for Morse and tight-binding potentials, respectively, as shown in Fig. 3.

Results and discussion

Nano-indentation process is simulated by four different models, i.e., MD model and CGMD models using Morse and tight-bonding potential functions, respectively. It is obvious that the tight-binding potential can provide a better prediction than the Morse potential. Results obtained by different models at three important instants of time, i.e., the equilibrium state, the instant of maximum deformation,

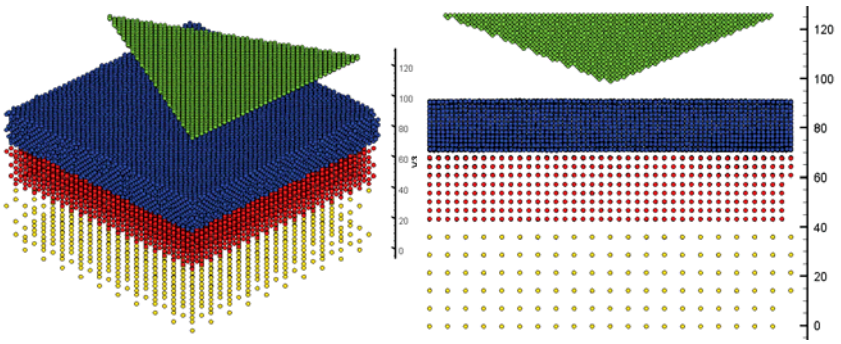

(a)

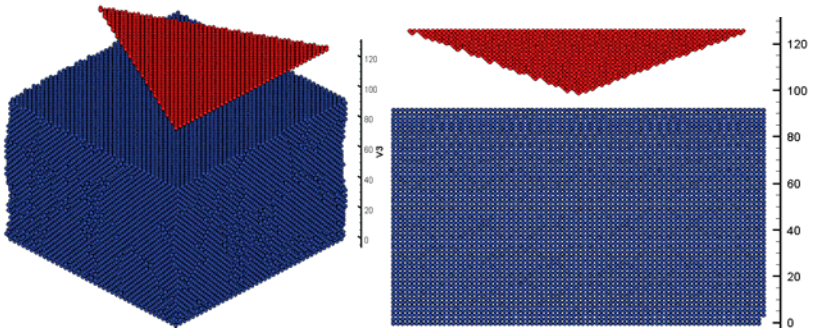

(b)

Figure 2: (a) CGMD and (b) all-atom MD simulation models of single crystal (100) Cu and diamond indenter

and the state after indentation, are compared to each other. When the indenter moves down and approached to the upper surface of substrate, oscillation of the atoms in the upper surface occurs especially near the probe tip. Moreover, some Cu atoms near the surface of the substrate jump up and are absorbed by the probe, called the phenomenon of jump to contact due to the attractive force between the atoms of the substrate and the indenter. When the probe tip continuously moves down and gradually penetrates into the substrate, the substrate starts to deform due to the repulsive force induced by the atoms of the probe. As the probe moves down further, both the contact area between the probe and the substrate and the repulsive force increase. The stress wave gradually extends from the upper side to the core region of the substrate. At this time a pile-up effect appears around the periphery of indent cave due to the occurrence of tensile force between atoms.

At the instant of maximum deformation, the stress wave tends to change its pattern from propagating isotropically to anisotropically along two sides only. Since the contact area of the probe and the substrate in the right side is larger than the

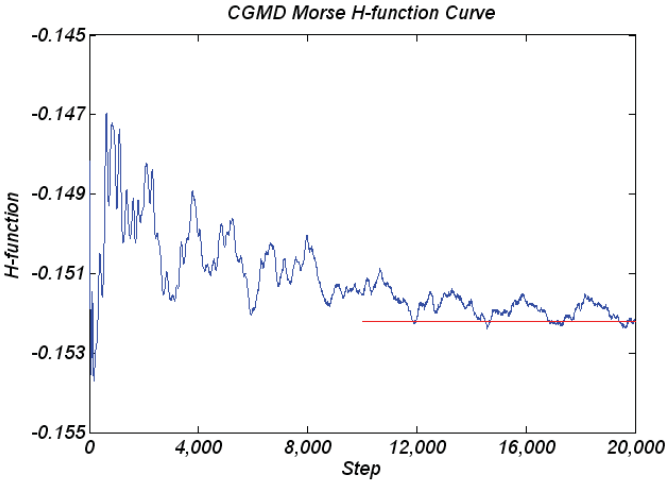

Figure 3: Variation of H-function with respect to number of time step for equilibrium run

left side due to geometric shape of the probe, as shown in the Fig.4, it can be found that the influence of the stress wave in the right side of the probe is more significant than the left side in both simulation results of MD and CGMD. Moreover, it is seen that the deformation and the dislocation patterns predicted by these two models are well consistent. They reveal the similar propagations along some specific slip directions. At this moment the wave propagation just beneath the probe tip becomes slow due to plastic deformation. After maximum deformation the probe starts to move up and then retract away from the substrate. The elastic strain energy is then gradually released and the dislocation lines finally appear on the slipping planes along some specific directions with the weakest bonding, as shown in the Fig. 5.

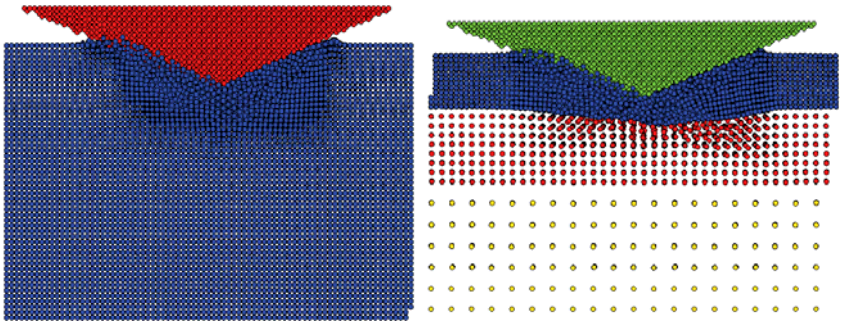

(a) (b)

Figure 4: Deformation patterns at the maximum indentation depth for simulation models of (a) all-atom MD and (b) CGMD using tight-binding potential

Fig. 6 shows the force-indentation depth curves for four different simulation

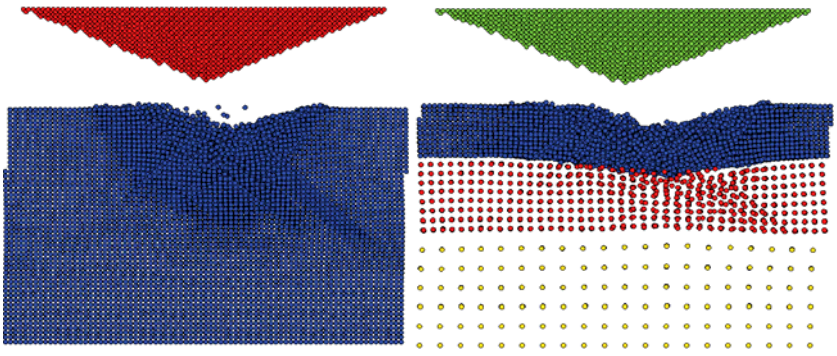

(a) (b)

Figure 5: Residual deformation patterns after unloading for simulation models of (a) all-atom MD and (b) CGMD using tight binding potential

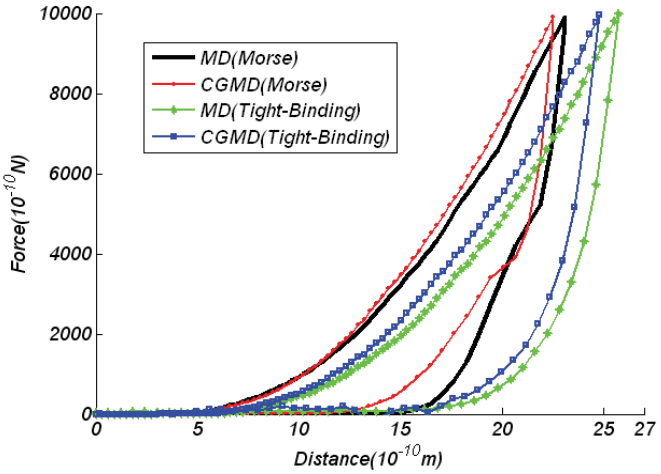

Figure 6: Force vs. indentation depth curves for four different simulation models

models. It is seen that the material using the Morse potential shows a harder stiffness than the tight-binding potential. Moreover, CGMD model behaves harder stiffness than MD model using the same potential. It was reported that at micro-/nanometer scales, materials exhibit size-dependent properties [17]. A typical example of this size-dependence is hardness. For instance, the hardness of (111) single crystal Cu and cold-worked polycrystalline Cu increases from less than 1 to about 2 GPa as the indentation depth decreases from 2000 to 150 nm [18]. Moreover, as the indentation depth decreases to the level about 30 nm, the hardness of Cu, deposited on the substrate of $LiNbO_3$, increases further to about 10 GPa [19].

Fig. 7 shows the variations of dynamic hardness versus the indentation depth

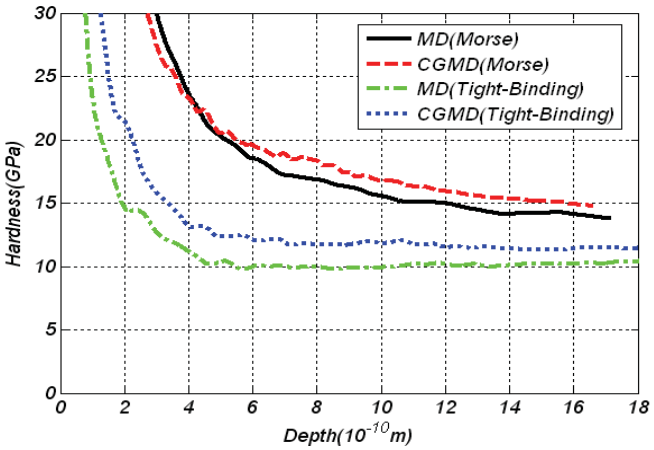

Figure 7: Variations of dynamic hardness versus indentation depth for four different simulation models

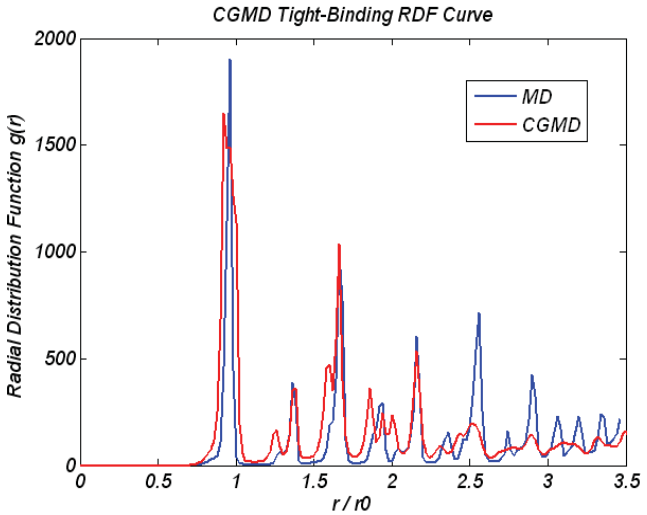

Figure 8: RDF simulated by Tight-bonding potential after unloading

for four different simulation models. It is seen that a similar trend of size-dependent hardness can also be observed in such a small scale from sub-nanometer to a few nanometers. The hardness predicted by the tight-binding and the Morse potentials shows a stable tendency as the indentation depth becomes more than 0.6 and 15 nm, respectively. Table 3 indicates the (a) Young's modulus and (b) hardness estimated by four different models. It was reported that the experimental Young's modulus for poly-crystal thin film copper is 135 GPa [19-20]. The hardness predicted by MD using Morse and tight-binding potentials is 13.8 and 10.5 GPa, respectively, while it is 14.7 and 11.5 GPa by CGMD using Morse and tight-binding potentials, re-

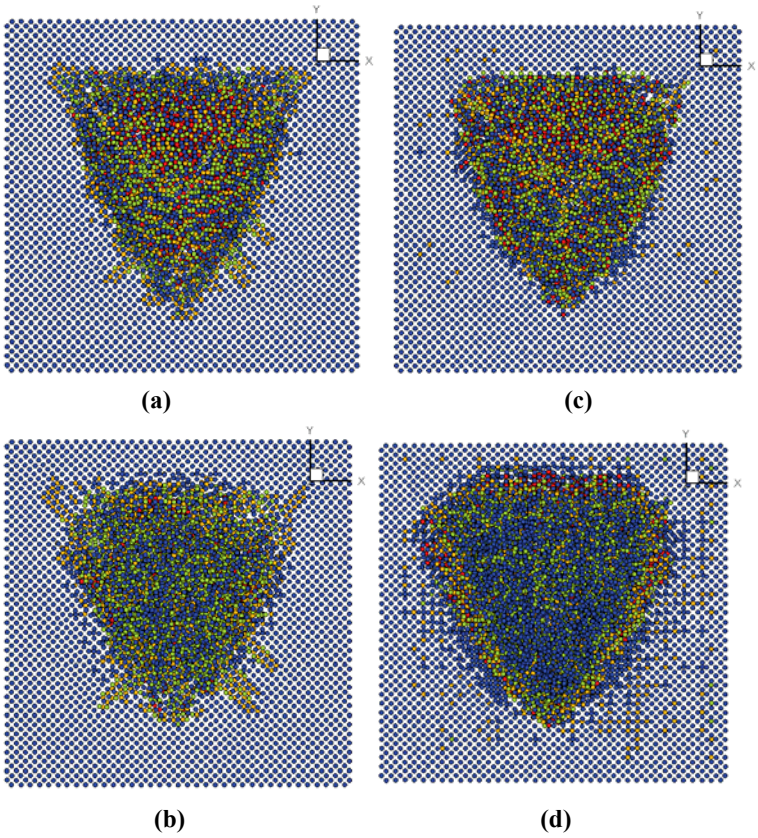

Figure 9: Top views (X-Y plane) on the surface of deformation region (a) at maximum loading and (b) after unloading predicted by Morse potential, as well as (c) at maximum loading and (d) after unloading predicted by tight-binding potential

spectively. On the other hand, the Young's modulus predicted by MD using Morse and tight-binding potentials is 275 and 263 GPa, respectively, while it is 302 and 289 GPa by CGMD using Morse and tight-binding potentials, respectively. It can be found that there exists no significant discrepancy between experimental data and simulation value in hardness; however, for Young's modulus, the experimental data is much lower than the simulation value. Moreover, compared to the experimental data, the tight-binding potential seems to provide a better result than the Morse potential. The discrepancy between CGMD and MD results for both hardness and Young's modulus using the same potential function is satisfactorily less than 10% in magnitude. In particular, the computational time of the former takes only 1/5 of the latter.

Fig. 8 shows the RDF simulated by tight-bonding potential after unloading. It

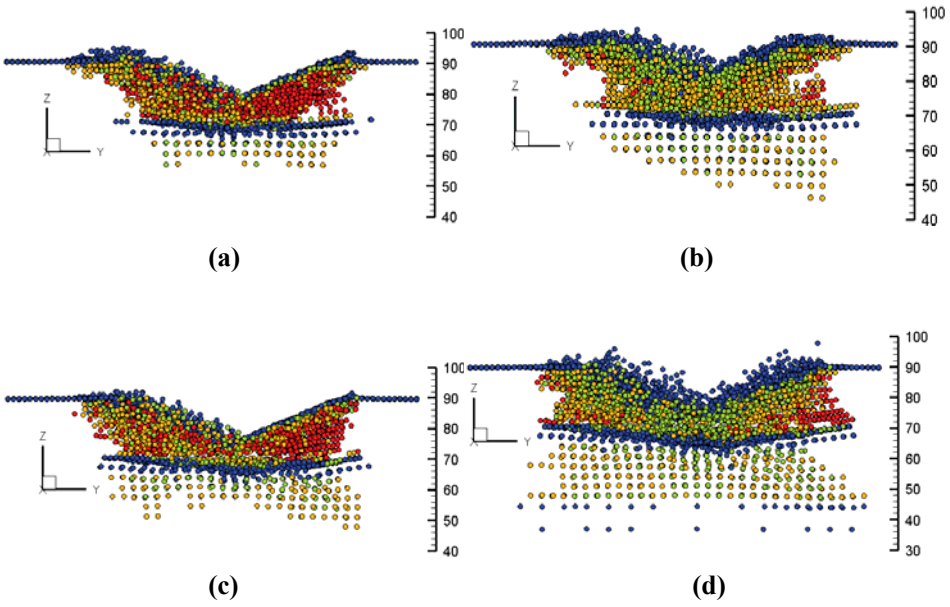

Figure 10: Side cross-sectional views (Y-Z plane) of deformation region (a) at maximum loading and (b) after unloading predicted by Morse potential, as well as (c) at maximum loading and (d) after unloading predicted by tight-binding potential

is seen that most of the peaks are consistent between MD and CGMD models. In other words, the real structure of atoms, evaluated by MD model, can also be satisfactorily described by CGMD model. Moreover, coordination number is adopted to trace and investigate the history of deformation. The normal coordinate number of Cu is twelve and can be disregarded. The other coordination numbers in the deformed region just underneath the indenter are marked by four different colors (CN = 8 as blue, CN = 9 and 10 as green, CN = 11 as yellow and CN > 12 as red). Blue atoms generally appear on the surfaces or the interfaces between adjacent layers with different lattices. Green and yellow atoms represent the regions subjected to tensile deformation to some extent, while the red atoms denote the regions subjected to compressive deformation. Fig. 9 shows the top views of deformation (a) at the instant of maximum loading and (b) after unloading, predicted by Morse potential as well as (c) at the instant of maximum loading and (d) after unloading, predicted by tight-binding potential, induced by the Berkovich tip on the top surface of substrate (X-Y plane). It is seen that the region of indent at the instant of maximum loading is smaller than that after unloading due to successive propagation of elastic wave. Fig. 10 shows the side cross-sectional views (Y-Z plane) of deformation region (a) at the instant of maximum loading and (b) after unloading, predicted by Morse potential as well as (c) at the instant of maximum loading and

(d) after unloading, predicted by tight-binding potential. The blue atoms at the top and the lower sides represent those located on the top surface and at the interface between atoms and CGMD1 nodes. At the instant of the maximum loading, as shown in the Figs. 10(a) and 10(c), significant compressive deformation, denoted by red color, can be seen just underneath the tip. Phenomenon of pile-up is also clearly exhibited. After unloading, as shown in Figs. 10(b) and 10(d), the depth of indent and region of compressive deformation are both significantly reduced due to elastic recovery. The region of residual deformation becomes deeper and wider. In addition, the deformation region predicted by tight-binding potential is slightly larger than that predicted by Morse potential. In other words, material using tight-binding potential behaves softer than Morse potential. It is worth to mention that the computational time required for CGMD model takes only about 1/5 of the all-atom MD model using the same potential function.

Conclusions

In this study, a simple and powerful method is proposed to derive the potential functions for different lattices of CGMD. The accuracy and reliability of these potential functions for CGMD are validated by comparing to the corresponding MD model through numerical simulation on nano-indentation process. Well consistent results can be found between MD and CGMD models in various aspects, such as force-displacement curves, deformation and dislocation patterns, characteristics of RFD, as well as the estimated material properties, such as hardness and Young's modulus. In particular, computational time can be significantly saved by using CGMD model without sacrifice of numerical accuracy. This study thereby provides a methodology to decrease the gap of size between atomic simulation and experimental work.

Acknowledgement

The authors gratefully acknowledge the support of the National Science Council of Taiwan, R.O.C. (Grant Nos. NSC 95-2221-E-006-273 and NSC 94-2212-E-006-048)

References

1. D. E. Kim, S. I. Oh, Nanotechnology **17** (2006) 2259.
2. J. Knap, M. Ortiz, J. Mech. Phys. Solids **49** (2001) 1899.
3. P. A. Klein, J. A. Zimmerman, J. Comput. Phys. **213** (2006) 86.
4. L. M. Dupuy, E. B. Tadmor, R. E. Miller, R. Phillips, Phys. Rev. Lett. **95** (2005) 60202.
5. E. B. Tadmor, M. Ortiz, R. Phillips, Phil. Mag. A **73** (1996) 1529.
6. V. B. Shenoy, R. Miller, E. B. Tadmor, D. Rodney, R. Phillips, M. Ortiz, J.

Mech. Phys. Sol. **47** (1999) 611.

7. E. B. Tadmor, M. Ortiz, R. Phillips, Philos. Mag. A **73** (1996) 1529.
8. E. B. Tadmor, R. Phillips, M. Ortiz, Langmuir **12** (1996) 4529.
9. R. E. Rudd, J. Q. Broughton, Phys. Rev. B **58** (1998) R5893.
10. R. E. Rudd, J. Q. Broughton, Phys. Status Solidi B **217** (2000) 251.
11. J. Q. Broughton, F. F. Abraham, N. Bernstein, E. Kaxiras, Phys. Rev. B **60** (1999) 2391.
12. D. J. Diestler, 2002 Phys. Rev. B **66** (2002) 184104.
13. Z. B. Wu, D. J. Diestler, R. Feng, X. C. Zeng, J. Chem. Phys. **119** (2003) 8013.
14. S. D. Chao, J. D. Kress, A. Redondo, J. Chem. Phys. **122** (2005) 234912.
15. F. Cleri, V. Rosato, Phys. Rev. B **48** (1993) 22.
16. L. A. Girifalco, V. G. Weizer, Phys. Rev. **114** (1959) 687.
17. J. M. Hailie, Molecular Dynamics Simulation Elementary Methods, John Wiley & Sons. Inc., New York, 1993.
18. T. Y. Zhang, W. H. Xu, J Mater. Res. **17** (2002) 1715.
19. K. W. McElhaney, J. J. Vlassak , W. D. Nix, J Mater. Res. **13** (1998) 1300.
20. T. F. Fang, W. J. Chang, Microelectro. Eng. **65** (2003) 231.
21. S. Suresh, T. G. Nieh, B. W. Choi, Scrip. Mater. **41** (1999) 951.
22. C. D. Wu, J. F. Lin, *Appl. Phys. A*, **91** (2008) 273.